Chemical Engineering Journal 246 (2014) 343–352

Contents lists available at ScienceDirect

Chemical Engineering Journal

journal homepage: www.elsevier.com/locate/cej

Comparison of Ni and Ni–Ce/Al_2O_3 catalysts in granulated and structured forms: Their possible use in the oxidative dehydrogenation of ethane reaction

J.P. Bortolozzi, T. Weiss, L.B. Gutierrez, M.A. Ulla *

Instituto de Investigaciones en Catálisis y Petroquímica, INCAPE (FIQ, UNL – CONICET), Santiago del Estero 2829, 3000 Santa Fe, Argentina

HIGHLIGHTS

- Ni and Ni–Ce/Al_2O_3 coatings on metallic foams were active and selective for the ODE.
- The cerium addition increased considerably the ethylene productivity.
- Catalytic features of the structured systems depend on the calcination temperature.
- The presence of chromium in the catalytic coatings mainly affects the selectivity.
- The structured systems showed higher ethylene productivity than powder catalysts.

GRAPHICAL ABSTRACT

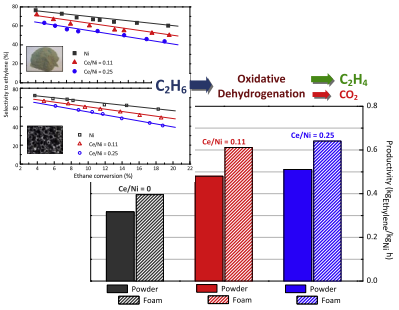

ARTICLE INFO

Article history:
Received 5 November 2013
Received in revised form 5 February 2014
Accepted 25 February 2014
Available online 12 March 2014

Keywords:
Structured catalysts
Metallic foams
Nickel oxide
Nickel–cerium oxides
Oxidative dehydrogenation of ethane

ABSTRACT

Ni and Ni–Ce/Alumina catalysts in structured form were prepared, characterized by different techniques and tested in the oxidative dehydrogenation of ethane (ODE). In order to gain further insight into active species, catalysts in granulated form were also synthesized, characterized and evaluated in the same reaction test.

The results indicated that the Ni and Ni–Ce/Al_2O_3 granulated catalysts were active and selective for this reaction. The addition of cerium using two atomic ratios (Ce/Ni = 0.11 and 0.25) significantly increased the ethylene productivity by kg of nickel mainly motivated by the marked increment in ethane conversion. This behavior could be explained by the smaller nickel oxide crystallite size and the incorporation of nickel into the ceria lattice.

The structured systems showed similar active species but achieved a better performance in terms of ethane conversion and ethylene productivity, compared with the granulated forms. The higher catalytic activity could be associated with the presence of lower crystallite sizes of the active phases and also related to a better utilization of active sites due to a higher accessibility of the reagents to the catalyst surface.

The existence of certain species (mainly chromium oxide) in the coverage also contributed to obtain higher conversion even though the selectivity to ethylene decreased. Lower temperature treatments applied to the structured support (550 °C instead of 700 °C) reduced the amount of these undesired species that favor the total oxidation of ethane.

* Corresponding author. Tel./fax: +54 342 4536861.
E-mail address: mulla@fiq.unl.edu.ar (M.A. Ulla).

http://dx.doi.org/10.1016/j.cej.2014.02.078
1385-8947/

1. Introduction

Ethylene is an important building block in the petrochemical industry. Today, it is mostly produced by naphtha or ethane cracking [1]. This process employs severe operating conditions and shows a number of disadvantages such as thermodynamical limitations and coke formation.

Among the alternative routes to produce ethylene, the oxidative dehydrogenation of ethane emerges as an attractive reaction because it presents several advantages, i.e. lower operating temperatures and the presence of oxygen to produce water as co-product, thus allowing overcoming thermodynamical limitations.

Numerous catalytic powder formulations were investigated for the oxidative dehydrogenation of ethane (ODE) in which vanadium was a traditional choice as active component [2]. However, in the last few years, nickel-based materials have become promising catalysts due to their capability to activate light paraffins at relatively low temperatures [3–5].

On the other hand, ceria presents particular chemical features such as its redox properties in the presence of transition metals [6–9] which makes it very attractive for applications in catalytic formulations in numerous reactions. The main role played by ceria is related to the generation of anionic vacancies and to the participation of reactive oxygen species, which can be tuned in the presence of other elements in the lattice [10,11]. The Ni–Ce combination has been studied for many reactions, e.g. the reduction of nitrogen oxides [12], reforming [13,14], partial oxidation [15,16] and redox reactions [17–19], among others.

The employment of a catalytic formulation in granulated form is difficult if a practical or industrial application is considered; therefore, it is important to take into account the feasibility of depositing them onto a substrate which constitutes a structured catalyst. These systems could provide numerous advantages inherent to their nature and morphological characteristics, although there are still unresolved issues that prevent their use in certain production processes.

Very few reports have been published in the literature on structured systems applied to the oxidative dehydrogenation reaction at low temperatures and most of them are mainly devoted to propane [20,21]. Therefore, the development of non-conventional reactor configurations leading to an increasing energy efficiency and the optimization of the reaction temperature control as well as to higher values of activity and/or selectivity looks like an interesting challenge.

Among the many options from which to choose substrates, metallic foams present remarkable features, i.e. the simplicity of building different structures and better heat transfer coefficients than those of the ceramic monoliths, which are useful for exothermal reactions [22]. In addition, the flow regime is turbulent allowing a better mixing of reagents and increasing axial and radial dispersion [23].

In this context, the aim of this work was the preparation, physicochemical characterization and catalytic evaluation of structured catalysts in the oxidative dehydrogenation of ethane reaction (ODE). The systems were prepared using AISI 314 stainless steel foams as substrates for Ni and Ni–Ce/Al_2O_3 catalysts. In order to gain further insight into active sites, catalysts in granulated form were also prepared, characterized by several techniques and evaluated in the same reaction test.

2. Material and methods

2.1. Granulated catalysts

Monometallic (Ni and Ce) and bimetallic (Ni–Ce) oxide catalysts were prepared by wet impregnation and co-impregnation, respectively, with a 15 wt% maximum loading. Alumina PURALOX Condea SBA-230 was used as support. Aqueous solutions of either nickel or nickel–cerium nitrates were used as metal precursors. In the mixture of these precursors, two different atomic ratios were used: Ce/Ni = 0.11 and 0.25. The solvent was removed by evaporation. The resulting granulated was oven dried for 8 h at 120 °C. Finally, it was calcined in air flow at 550 °C for 4 h.

2.2. Structured catalysts

AISI 314 stainless steel cylinder foams (*Porvair*®, 60 ppi, diameter ~10 mm and height ~20 mm) were treated in a muffle at 900 °C for 2 h. The γ-Al_2O_3 support (*Nyacol*® AL20DW) was deposited by vacuum-assisted immersion. Further details were given elsewhere [24]. In order to investigate the influence of calcination temperature, the structured supports were calcined in static air at 550 °C or 700 °C for 2 h. Solutions (0.43 M) of the metallic oxide precursors (nickel and cerium nitrates) were used to incorporate the active metallic oxides to the alumina coating by cycles of immersion – blowing – drying (120 °C, 1 h) – calcination (550 °C, 4 h). This cycle was repeated until the final metal oxide loading of ~15 wt% was achieved. The structured catalysts were prepared under the form of Ni and Ni–Ce oxides. For the latter, the precursor solutions were prepared with Ce/Ni atomic ratios 0.11 and 0.25. The catalysts were named as indicated in Table 1.

2.3. Catalysts characterization

Crystalline phases of the different granulated catalysts were studied by X-ray diffraction (XRD). The analysis was performed with a Shimadzu XD-D1 diffractometer. Diffraction patterns were recorded using Cu Kα radiation over a 20–85° range at a scan rate of 1°/min, operating at 30 kV and 40 mA. The software package of the equipment was used for the phase identification. The estimated size of nickel oxide crystallite was calculated by the Scherrer equation. The plane used for the calculation of the crystallite size of nickel oxide was (200), corresponding to the main peak of NiO at 43.3° while for the calculation of cerium oxide crystallite the plane (111) corresponding to the main peak of CeO_2 at 28.6° was considered. The calculated values are an average of three FWHM measurements of the corresponding peaks in different XRD patterns.

The reducibility of nickel and cerium species for the granulated samples was analyzed by temperature-programmed reduction (TPR). The experiments were performed in an Ohkura TP-2002S instrument using a mixture of H_2/Ar (5%) as reducing gas. The heating rate was 10 °C/min from room temperature to 900 °C.

X-ray photoelectron spectroscopy (XPS) measurements were performed with a multitechnique equipment (SPECS) with a dual Mg/Al X-ray source and a hemispherical PHOIBOS 150 analyzer operating in the fixed analyzer transmission (FAT) mode. The spectra were obtained with a pass energy of 30 eV and Mg Kα X-ray source power of 200 W. The pressure in the analyzing chamber was less than 5.9×10^{-7} Pa. The spectral regions corresponding to Ni 2p, Ce 3d and C 1s core levels were recorded for each sample. Peak fitting was performed with the CASAXPS software. The peak areas were determined by integration employing a Shirley-type background. Peaks were considered to be a mixture of Gaussian and Lorentzian functions.

The Raman spectra were recorded using a LabRam spectrometer (Horiba-Jobin–Yvon) coupled to an Olympus confocal microscope (a 100 × objective lens was used for simultaneous illumination and collection), equipped with a CCD detector cooled to about −70 °C using the Peltier effect. The excitation wavelength was in all cases 532.13 nm (Spectra Physics diode pump solid state laser). The laser power was set at 30 mW.

Table 1
Main features of the prepared catalytic systems.

Catalyst[a]	Metal loading (wt%)	Ce/Ni atomic ratio[b]	Crystallite size NiO (nm)[c]	Crystallite size CeO_2 (nm)[d]
Ni (P)	15.0	–	12.4	–
Ni (S) – C700[e]	14.7	–	–	–
Ni (S) – C550[e]	15.4	–	–	–
NiCe 0.11 (P)	15.0	0.11	9.1	4.4 (3.7)
NiCe 0.11 (S) – C700	16.0[f]	0.11	–	–
NiCe 0.11 (S) – C550	15.1[f]	0.11	–	(3.1)
NiCe 0.25 (P)	15.0[f]	0.25	<9.1	6.1 (4.6)
NiCe 0.25 (S) – C550	16.1[f]	0.25	–	(4.1)

[a] P: Powder form – S: Structured form.
[b] Atomic ratio in the precursors solution.
[c] Estimated by the Scherrer equation.
[d] Estimated by the Scherrer equation. Between brackets is value calculated by Raman Spectroscopy.
[e] Calcination temperature of the support: C700 = 700 °C and C550 = 550 °C.
[f] Referred to NiO.

The morphology and distribution of the catalytic coatings were characterized by Scanning Electron Microscopy (SEM) JEOL JSM 35C operating at 20 kV, equipped with EDX energy-dispersive system. Semi-quantitative results were obtained with the theoretical quantitative method (SEMIQ) of the EDX software. For the chemical elemental analysis (EDX), the samples were attached with graphite tape onto the sample holder. X-ray spectra were acquired with an accelerating voltage of 20 kV. The sample coating procedures were performed using a combined carbon deposition of metal SPI Supplies 12157-AX under argon atmosphere.

A Testlab TB04 ultrasound bath equipment (40 kHz and 160 W) was used to carry out the mechanical stability tests of the catalytic coatings. The weight loss percentage was determined after exposing the samples to an ultrasound bath in acetone at 25 °C for 1 h.

2.4. Catalytic tests

The oxidative dehydrogenation of ethane was carried out in a flow system in a temperature range between 300 and 450 °C. The mass of the catalysts used was about 400 mg and the final flow was fixed to achieve a constant W/F value of 0.48 g s/cm^3.

The granulated catalysts (100–120 mesh) were introduced into the reactor (diameter ≈ 15 mm) with a catalytic bed volume similar to that of the structured systems.

The feed composition was 6% O_2 and 6% C_2H_6 diluted in He. Reactants and products were analyzed with a Shimadzu GC 2014 gas chromatograph equipped with a packed column (HayeSep D).

No carbon monoxide was detected downstream after the reactor. Closure of the carbon mass balance was 100 ± 2%. The conversion of ethane ($X_{C_2H_6}$) and the selectivity toward ethylene ($S_{C_2H_4}$) were based on the carbon mass balance and were calculated as follows:

$$X_{C_2H_6} = \frac{[CO] + [CO_2] + 2[C_2H_4]}{2[C_2H_6]} \times 100$$

$$S_{C_2H_4} = \frac{2[C_2H_4]}{[CO] + [CO_2] + 2[C_2H_4]} \times 100$$

The productivity of ethylene was given by the following equation:

$$P = F_{C_2H_6} \times X_{C_2H_6} \times S_{C_2H_4} \times 28/W_{Ni}\ (\text{or } W_{cat}), [\text{kg}_{C_2H_4}/\text{kg}_{Ni}\ (\text{or kg}_{cat})\ \text{h}]$$

where $F_{C_2H_6}$ is the flow rate of ethane in mol/h, 28 (g/mol) is the molecular mass of ethylene and W_{Ni} or W_{cat} is the mass of Ni or catalyst (support + active phase) expressed in kg.

3. Results

In order to study the catalytic species present on the coatings deposited onto the stainless steel foams and their interaction with the substrate, a comparison with the corresponding granulated catalysts was performed. Several techniques such as XRD, TPR, XPS and LRS were applied to study the catalysts under their granulated form with the aim of gaining further information into the species on the surface of the catalysts. Through these studies, substantial assignments to the Raman bands were able to be carried out.

3.1. Metal oxide sites characterization: granulated catalysts

3.1.1. X-ray diffraction (XRD)

Fig. 1 shows the X-ray diffraction patterns of the granulated catalysts. Characteristic peaks of alumina (Fig. 1a) (JCPDS 10-425) and nickel oxide (NiO) at 2θ = 37.3°, 43.3°, 62.9°, 75.5° and 79.6° (JCPDS 47–1049) were observed in all samples. The presence of NiO diffraction signals indicates the saturation of the support surface covering the monolayer and the incipient formation of three-dimensional species. The crystallite size was estimated in 12.4 nm, 9.1 nm and <9.1 nm for catalysts Ni (P), NiCe 0.11 (P) and NiCe 0.25 (P), respectively (Table 1).

Additional peaks assigned to cerium oxide (CeO_2), located at 2θ = 28.6°; 33.1°; 47.5°; 56.4°; 59.1°; 69.5°; 76.8° and 79.1° (JCPDS

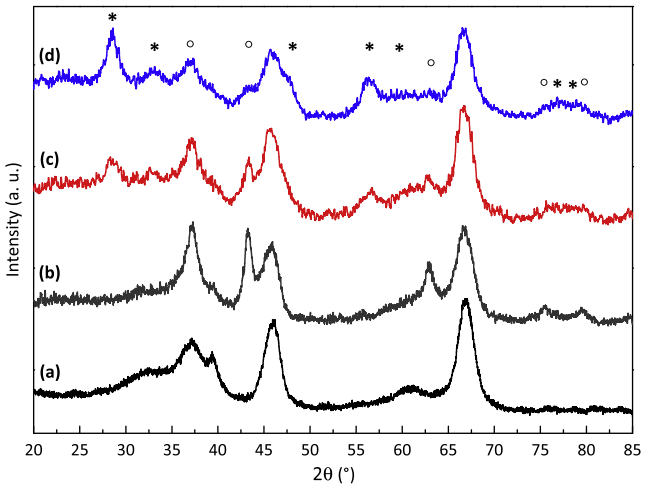

Fig. 1. XRD patterns of the granulated catalysts: Al_2O_3 (a), Ni (P) (b), NiCe 0.11 (P) (c) and NiCe 0.25 (P) (d). Symbols: ° NiO; ∗ CeO_2.

43–1002) were indentified in both cerium-promoted catalysts (NiCe 0.11 (P) and NiCe 0.25 (P)). The full width at half height of the peaks decreased as the amount of cerium increased, indicating an increase in the size of the crystalline domain of the ceria phase. Crystalline domain sizes estimated for these species were 4.4 and 6.1 nm for the formulation with the lowest and the highest amount of promoter, respectively (Table 1).

3.1.2. Temperature-programmed reduction (TPR)

The temperature-programmed reduction of the three samples confirmed the presence of NiO with different support interactions (Fig. 2). The Ni (P) reduction profile (Fig. 2a) shows a small peak in the 300–390 °C temperature range, corresponding to 3-D nickel oxide reduction and a broad peak at higher temperature, associated with the reduction of Ni species highly dispersed and with a strong interaction with the alumina.

The changes observed in the reduction profile of the catalyst with Ce/Ni = 0.11 atomic ratio (Fig. 2b) are (i) an additional peak in the 200–300 °C region, associated with weakly adsorbed oxygen species and (ii) a marked shift of the main peak towards high reduction temperature values (∼50 °C).

In the NiCe 0.25 (P) profile (Fig. 2c), the area of the peak at low temperature is larger than in the NiCe 0.11 (P) catalyst and the maximum temperature associated with the reduction of Ni cation with a strong interaction with the support, increases approximately 65 °C compared with the catalyst without the promoter. So, in this catalyst, the presence of adsorbed oxygen species would be more significant than in the Ce/Ni = 0.11 sample.

3.1.3. X-ray photoelectron spectroscopy (XPS)

The XPS spectra of the catalysts are shown in Fig. 3. The Ni (P) spectrum shows the Ni $2p_{3/2}$ main signal located at 856.0 eV with the satellite at higher binding energy (BE) (Table 2). The corresponding binding energies are assigned to Ni^{2+} with a strong interaction with the support, located in octahedral coordination [25]. This interpretation is supported by the fact that bulk NiO presents a lower binding energy (854.5 eV) and shows a difference between the Ni $2p_{3/2}$ and Ni $2p_{1/2}$ main peaks of about 18.6 eV [26].

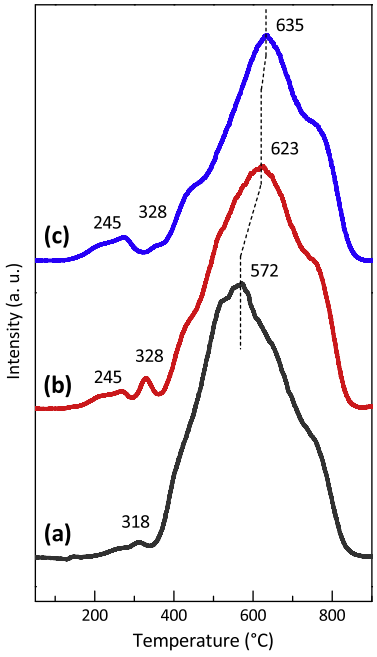

Fig. 2. Reduction profiles of the granulated catalysts: Ni (P) (a), NiCe 0.11 (P) (b) and NiCe 0.25 (P) (c).

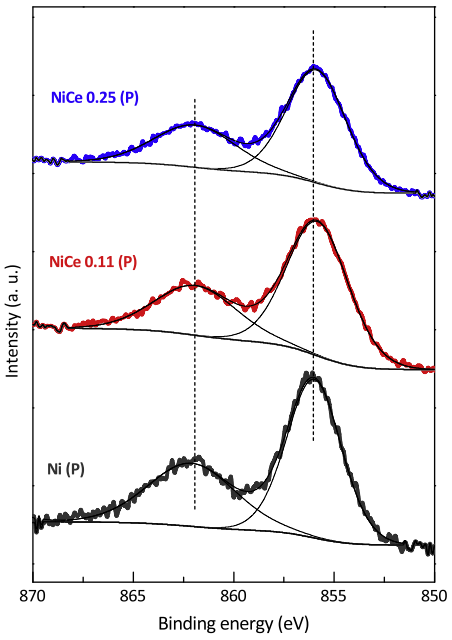

Fig. 3. XPS spectra of the granulated catalysts: Ni $2p_{3/2}$.

Table 2
Ni 2p binding energy (BE) of the powder catalysts.

Catalysts	Energy region	BE (eV) (width)
Ni (P)	Ni $2p_{3/2\ main}$	856.0 (3.15)
	Ni $2p_{3/2\ sat}$	862.1
NiCe 0.11 (P)	Ni $2p_{3/2\ main}$	855.8 (3.59)
	Ni $2p_{3/2\ sat}$	861.9
NiCe 0.25 (P)	Ni $2p_{3/2\ main}$	855.9 (3.62)
	Ni $2p_{3/2\ sat}$	861.9

In the case of Ni (P), that difference is 17.6 eV, suggesting that the nickel would be located on the surface as a spinel-type structure.

The same tendencies are visualized on the Ni $2p_{3/2}$ spectra of both bimetallic oxide catalysts (Table 2). Moreover, the widths of these Ni $2p_{3/2}$ main signals are larger than that of the Ni (P), suggesting that the formers could contain the contribution of two types of surface Ni^{2+} due to the different interaction with Al_2O_3 and/or CeO_2.

Neither signals of Ni $2p_{1/2}$ nor signals of Ce $3d_{5/2}$ in the 870–895 eV region could be properly differentiated since they overlapped.

3.1.4. Laser Raman Spectroscopy (LRS)

Fig. 4a shows the Raman spectra of the granulated catalysts. The monometallic oxide catalyst shows a broad and asymmetrical band at 500–550 cm^{-1} region corresponding to the stretching of Ni–O bond (first order phonons). The location of this band, which shifted to higher frequencies with respect to the bulk nickel oxide, is associated with a strong interaction between the Al_2O_3 support and the nickel species, in agreement with TPR and XPS results [27]. A small shoulder at ∼400 cm^{-1} assigned to material surface vacancies and weak bands at 700 and 1080 cm^{-1} associated with second order phononic modes of nickel oxide were also present [28]. No specific signals at 370, 598 and 760 cm^{-1} corresponding to crystalline (bulk) $NiAl_2O_4$ were observed, thus confirming the absence of this phase [29].

Cerium-containing catalysts NiCe 0.11 (P) and NiCe 0.25 (P) showed the same Ni–O stretching bands, although this signal

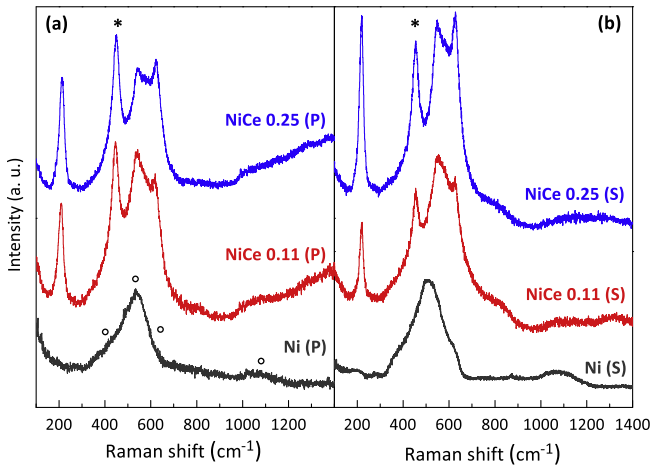

Fig. 4. Laser Raman spectra of the granulated (a) and structured catalysts (b). Symbols: ° Ni–O; ∗ Ce–O.

showed a marked shift (~12 cm^{-1}) towards higher frequencies (Fig. 4a).

In addition, an intense signal at ~465 cm^{-1} corresponding to CeO_2 fluorite-type structure was observed. This signal is related to the oxygen atoms vibration around Ce^{4+} cation, denominated "breathing mode" [30]. Furthermore, additional sharp bands at 224 and 632 cm^{-1} (Fig. 4a) are assigned with a strong nickel–cerium interaction. The former band could also be associated with the crystallite size of ceria (surface phonon modes on the nanocrystals). However, this band is expected at higher frequency (~270 cm^{-1}) and it should be coupled with another high intensity signal located at ~315 cm^{-1}, which is absent in the spectra [31]. These observations confirm that the addition of cerium leads to a significant change in the structure of the cerium-promoted solids, in good agreement with previous results.

Graham et al. [32] proposed a simple and empirical equation to calculate approximately the sizes of CeO_2 crystallites, as shown in Eq. (1):

$$d = \frac{b}{(\mathrm{FWHM} - a)} \quad (1)$$

where d is the crystallite size in Å, FWHM is Full Width at Half Maximum in cm^{-1} and a, b are constants equal to 10 and 1036, respectively.

For both promoted samples, the signal shows a considerable width (~35–40 cm^{-1}) supporting the hypothesis about the presence of crystallites with dimensions close to few nanometers. The estimated sizes with Eq. (1) were 3.7 nm and 4.6 nm for NiCe 0.11 (P) and NiCe 0.25 (P) (Table 1).

These values are somewhat lower than those calculated with the Scherrer equation, but they have identical trend. Kanakaraju et al. reported results about cerium oxide films and they found that the crystallite sizes calculated by X-ray diffraction are higher than those obtained from the Raman spectra [33]. Recently, Bourja et al. investigated the CeO_2 nanoparticles dehydration process by applying high temperature treatments [34]. This process leads to the elimination of intercrystalline water and OH^- ions and causes a lattice contraction with disorder in the solid structure. In that report, the authors calculated the crystallite size of nanoparticles with both techniques and compared the results. They concluded that the differences are justified since the model for crystallite size estimation from Raman spectra does not include the above mentioned structural changes.

3.2. Metal oxide sites characterization: structured catalysts

The metal oxides characterization of the structured catalysts was performed by Laser Raman Spectroscopy (LRS), Scanning Electron Microscopy (SEM) and Energy-Dispersive X-ray Analysis (EDX). The former technique is very useful because it allows analyzing the oxide species present on the foam surface. Starting from previous knowledge on the active sites present on the alumina-based granulated catalysts, it is easier to understand which species are present on the structured systems surface.

3.2.1. Laser Raman Spectroscopy (LRS)

Fig. 4b shows the Laser Raman spectra of the structured catalysts. The Ni–O species signals (400–450, 550, 700 and 1080 cm^{-1}) are observed in the Raman spectra of all structured systems (Fig. 4b). Therefore, nickel species similar to those present in the granulated samples were formed.

In the spectra of the cerium-promoted system, a sharp, intense band assigned to Ce–O (~460 cm^{-1}, fluorite) can be identified, which indicates oxide formation. The additional bands at 224 and 632 cm^{-1} can also be clearly observed. In this way, it can be assumed that cerium species similar to those of the granulated samples are also formed on the coating surface.

The crystallite sizes estimated with Eq. (1) were 3.1 and 4.1 nm for the Ce/Ni = 0.11 and 0.25, respectively (Table 1). These values are lower than those calculated for the granulated catalysts, suggesting smaller crystalline domains in the surface of structured systems.

3.2.2. Chemical characterization

The atomic ratios of the components in the coverage (Ni, Al, Ce and Cr) were analyzed by the EDX technique. Table 3 shows the results of the most representative components of the coated foams. Relative concentrations of Ni, Al, Ce and Cr are reported because these are the main elements which are present in the catalytic systems.

The presence of aluminum in all sectors confirms the correct distribution of the support (Al_2O_3) onto the foam walls. The marked enrichment of nickel compared to the treated substrate indicates that the quantified Ni corresponds to the active phase.

The Ni/Al ratio in both cerium-free catalysts was close to the metal/support ratio present in the granulated samples. This tendency was also observed in the cerium-promoted samples. The Ce/Ni = 0.11 sample showed that the Ce/Ni ratio on the foam surface was in agreement with the used proportion in the solution of the metallic oxide precursors. These observations show a reasonably homogeneous distribution of the active components on the foams surface.

On the other hand, the Cr/Ni and Cr/Al ratios showed a marked increment when the calcination temperature of the support was 700 °C instead of 550 °C. The thermal treatment temperature seems to affect the catalytic layer composition through the migration of chromium species from the substrate (Table 3).

Table 3
EDX results of the most representative elements on the catalytic coatings.

Catalyst	Atomic ratio			
	Ni/Al	Ce/Ni	Cr/Ni	Cr/Al
Ni (S) – C700	0.14 ± 0.02	–	0.08 ± 0.03	0.010 ± 0.003
Ni (S) – C550	0.17 ± 0.02	–	0.03 ± 0.01	0.005 ± 0.002
NiCe 0.11 (S) – C700	0.11 ± 0.01	0.14 ± 0.02	0.11 ± 0.04	0.012 ± 0.004
NiCe 0.11 (S) – C550	0.16 ± 0.02	0.13 ± 0.02	0.05 ± 0.03	0.006 ± 0.002
NiCe 0.25 (S) – C550	0.16 ± 0.02	0.25 ± 0.03	0.05 ± 0.02	0.007 ± 0.001

3.2.3. Morphology and mechanical stability

The as received foams were calcined in air at 900 °C for 2 h for the stabilization and conditioning of the walls surfaces, generating roughness and thereby promoting a better anchoring of the catalytic coating. By immersion in the support colloidal suspension, a homogeneous layer of γ-Al_2O_3 deposited onto the walls of the substrate was obtained.

After the drying process some small cracks with micrometer sizes (<1 μm) were observed, mainly in the outer layer of the coating (Fig. 5). The temperature of the calcination treatment (550 °C or 700 °C) did not significantly affect the morphology of the Al_2O_3 layer. The coating calcined at lower temperature looks similar to the one calcined at 700 °C [35].

The adhesion of the coated catalysts was examined by submitting the structured systems to an ultrasound treatment (see Experimental section). Catalytic coatings deposited on treated foams showed high adherence. The mass loss (percentage relative to the total mass of the system) was less than 1.50 wt% after 60 min of exposure. If the weight loss were referred only to the catalytic coating, these values would rose up to a maximum of ~7.00 wt% also demonstrating an acceptable adherence. However, these values could result lower because some small parts of the foam struts were detached after the ultrasonic treatment.

On the other hand, the adhesion of the catalytic coating treated at 550 °C was slightly lower than that of the sample calcined at 700 °C, but this difference was not significant (Fig. 6).

3.3. Catalytic behavior for the oxidative dehydrogenation of ethane

Fig. 7 shows ethane conversion at different temperatures for the prepared catalysts. In all cases, a moderate conversion was achieved. Nevertheless, the incorporation of cerium to the Ni formulation significantly improved the catalytic activity and similar conversion levels were obtained but at lower temperatures (~30 °C), indicating that the activation of ethane on the catalytic surface takes place at lower temperature. Besides, all structured systems show an increase in the conversion values, compared with the corresponding granulated formulation. However, the conversion was not significantly modified by the treatment temperature (Fig. 7).

The results of the ethylene selectivity as a function of temperature for Ni–Ce granulated catalysts showed that the presence of cerium led to a slightly more marked dependence on temperature

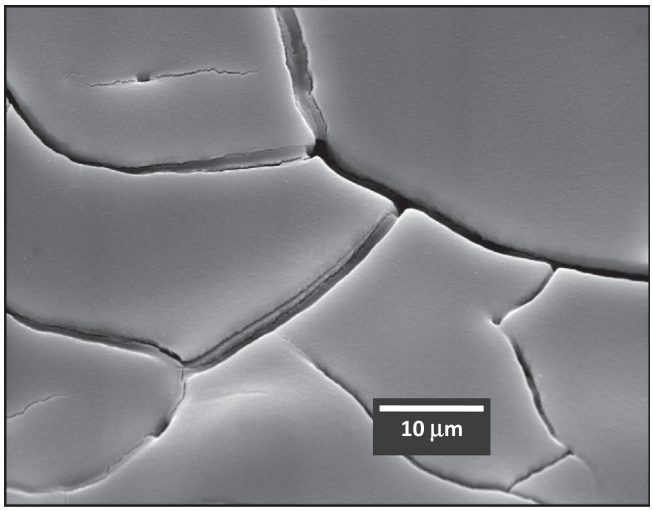

Fig. 5. SEM micrograph of the catalytic coating (Al_2O_3 layer calcined at 550 °C for 2 h).

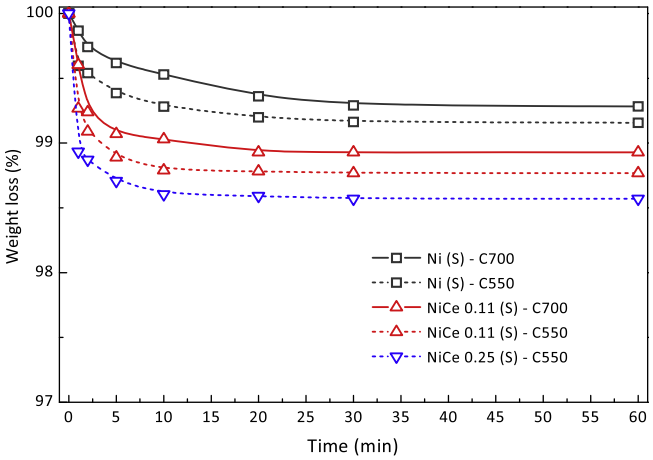

Fig. 6. Adherence tests: catalytic coatings. Al_2O_3 layer calcined at 550 °C (dotted line) and at 700 °C (solid line).

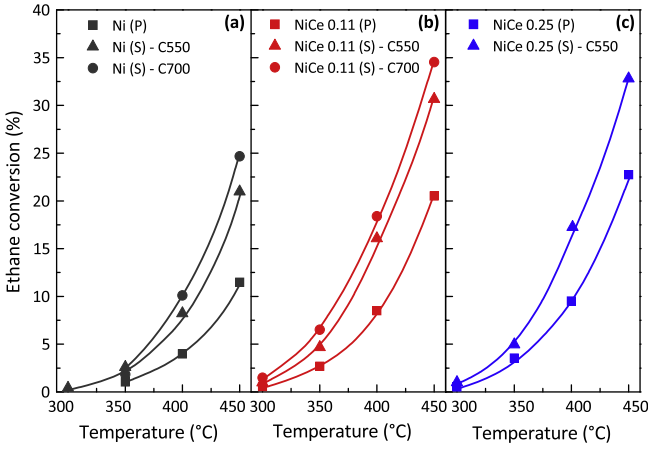

Fig. 7. Ethane conversion of the catalytic systems: Ni (a), Ce/Ni = 0.11 (b) and Ce/Ni = 0.25 (c). Reaction conditions: W/F = 0.48 g s/cm^3, C_2H_6/O_2 = 1.

(and ethane conversion) increment, in comparison with cerium-free formulations (Table 4). At the same time, granulated solids showed a higher selectivity to ethylene in comparison with the structured systems, mainly when the support was calcined at 700 °C (Table 4).

On the other hand, the selectivity to ethylene of the granulated and structured catalysts evaluated at constant temperature (T = 400 °C) and varying the W/F ratio is shown in Fig. 8. As a general remark, the prepared catalysts show a decrease with increasing conversion in the range from 2% to 22%, suggesting that the oxidation of ethylene occurs to some extent. Besides, at the same conversion level, the structured systems show a barely lower selectivity compared with the corresponding granulated sample (Fig. 8a and b).

Although the selectivity of the Ni (S) – C550 structured catalyst was similar to that of the NiCe 0.11 (S) – C550 and NiCe 0.25 (S) – C550 samples and they showed the same trend, the former system presents a slightly less pronounced decrease with increasing the ethane conversion (Fig. 8b). A similar behavior was also found in the granulated catalysts (Fig. 8a). These results indicate that the ethylene total oxidation is somewhat more favored in the cerium-containing formulations than in the promoter-free catalysts.

In order to evaluate the global catalytic behavior at a fixed temperature, the ethylene productivity by kg of nickel and kg of catalyst was calculated (Fig. 9). The results show that the ethylene

Table 4
Catalytic behavior of the catalysts as a function of temperature. Reaction conditions: T = variable, W/F = 0.48 g s/cm^3, C_2H_6/O_2 = 1.

Catalyst	350 °C		400 °C	
	Conversion (%)	Selectivity (%)	Conversion (%)	Selectivity (%)
Ni (P)	1.1	76.8	4.0	76.5
Ni (S) – C700	1.9	35.9	10.1	34.3
Ni (S) – C550	2.6	68.0	8.2	67.1
NiCe 0.11 (P)	2.7	67.5	8.5	61.9
NiCe 0.11 (S) – C700	6.5	35.0	18.4	31.0
NiCe 0.11 (S) – C550	4.7	61.1	16.1	51.3
NiCe 0.25 (P)	3.5	63.6	9.5	51.9
NiCe 0.25 (S) – C550	5.0	55.9	17.3	44.5

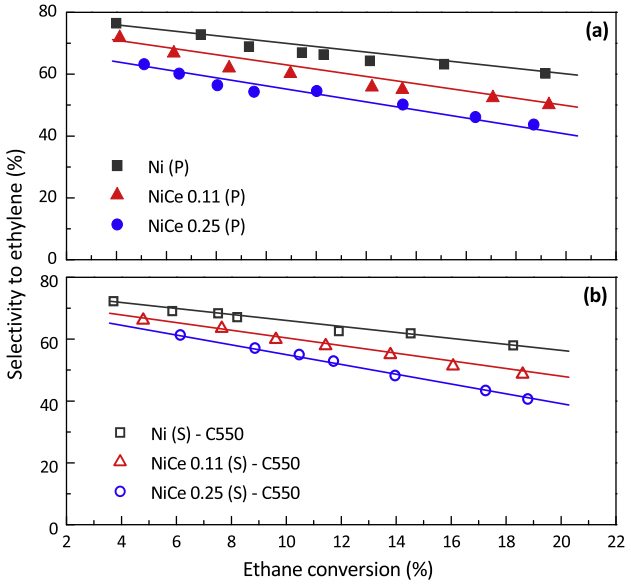

Fig. 8. Selectivity to ethylene at fixed temperature for the catalysts. Reaction conditions: T = 400 °C, W/F = variable, C_2H_6/O_2 = 1.

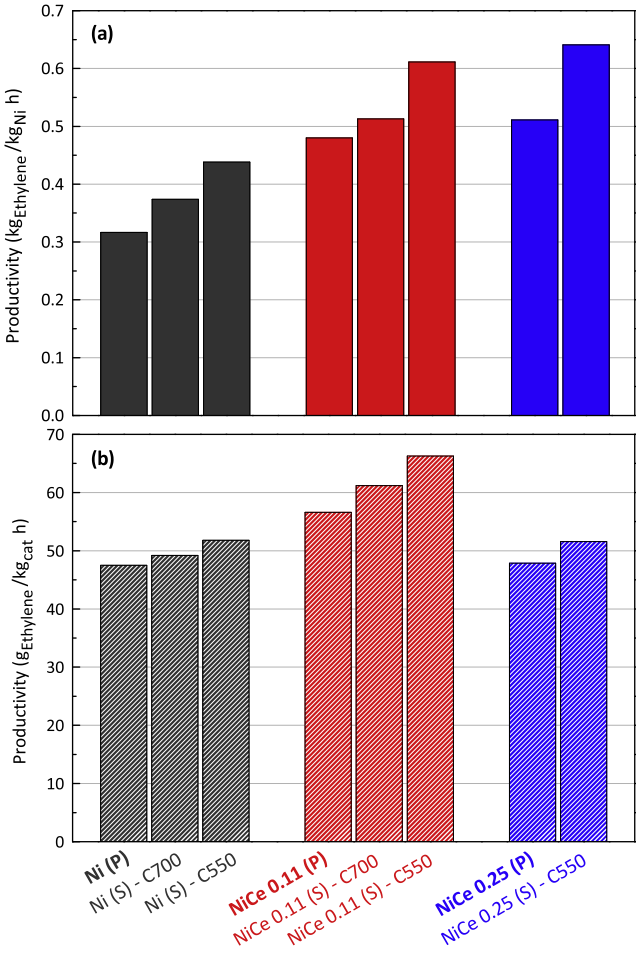

Fig. 9. Ethylene productivity of the catalysts. Reaction conditions: T = 450 °C, W/F = 0.48 g s/cm^3, C_2H_6/O_2 = 1.

productivity is enhanced with the addition of cerium at 450 °C (Fig. 9a). The incorporation of the promoter in both low and high loading (NiCe 0.11 (P) and NiCe 0.25 (P)) resulted in an increase of the global performance considered by kg of nickel. If the productivity is expressed by kg of catalyst (Fig. 9b), the formulations with Ce/Ni = 0.11 ratio show the best values, suggesting the existence of an optimal Ce/Ni ratio which maximizes the performance. Structured systems showed, in all cases, a higher productivity than the corresponding granulated formulation. In addition, it is noteworthy to mention that the results obtained for the other reaction temperatures analyzed (300, 350 and 400 °C) showed the same trend.

4. Discussion

4.1. Features of the active sites

The results obtained after a detailed characterization of the granulated catalysts are essentially useful to recognize the metal oxide species present on the catalytic coatings onto metallic foams. Therefore, the LRS assignments and the chemical information obtained from EDX, both of them applied to the structured catalysts, may shed light on the catalytic oxide species present on the coverage.

Through XRD results, the presence of nickel and cerium oxides was verified. Solsona et al. [19] reported that the presence of cerium limited the growth of the nickel oxide crystallite, as observed in the NiCe (P) samples studied. The addition of cerium produced a decrease in the crystalline domain of NiO: from 12.1 nm to <9 nm for the Ni (P) and the NiCe 0.25 (P) samples, respectively (Table 1).

Taking into account that the ionic radius of the Ni^{2+} cation (0.69 Å) [36] is smaller than that of Ce^{4+} (0.97 Å) [37], it is possible that a portion of nickel may be incorporated into the ceria without modifying its fluorite structure, as reported by Shan et al. and Deraz [38,39].

The presence of NiO and CeO_2 and their strong interaction was also confirmed by XPS and TPR. The former confirmed the absence of bulk nickel oxide in the surface of the catalysts whereas the latter technique also showed the existence of reducible species in the range of 200–300 °C. These species would result from the incorporation of small amounts of Ni into the CeO_2 network, leading to the formation of a solid solution Ni–Ce–O, capable of both generating

anionic vacancies and adsorbing oxygen. Besides, they present high reactivity and they are reduced at low temperatures yielding the peak observed at ~245 °C [19,40–42].

The reduction temperature shift of the main peak indicates that there are also some nickel species with different reducibility. The incorporation of the cations Ni^{2+} into the ceria lattice leads to a more difficult reduction process [38]. Consequently, the presence of cerium could generate new species, which might modify the nickel active site surroundings.

Furthermore, the marked shift in the reduction temperature of the former sample could be related to the formation of a major amount of solid solution or to an increase in the amount of nickel that was incorporated into the ceria structure. Therefore, a larger number of anionic vacancies could be formed.

According to the Raman spectra, the presence of the new signals in cerium-promoted catalysts (224 and 632 cm^{-1}) can be directly related to the oxygen network distortions [42], demonstrating that the incorporation of the Ni^{2+} cation into the ceria lattice occurred to some extent, with the consequent generation of oxygen vacancies.

Moreover, the shift (~3–4 cm^{-1}) of the CeO_2 main signal towards lower frequencies is also indicative of a change in the crystal lattice parameters and the presence of oxygen vacancies. At the same time, the width of this main signal is related to the crystalline domain size of cerium oxide, both being inversely proportional. Through X-ray diffraction, Laser Raman Spectroscopy and mainly EXAFS, Vlaic et al. concluded that the introduction of a cation with a smaller ionic radius than that of cerium into the CeO_2 network modifies the structure, leading to a shortening of the Ce–O bond. However, the cerium atoms coordination and fluorite-type structure remain unaltered [43].

The relative intensity of these two signals at 224 and 632 cm^{-1} was higher in the sample with the Ce/Ni = 0.25 ratio, suggesting that a greater quantity of solid solution was formed or a higher amount of nickel entered into the crystalline structure of cerium oxide in this sample, in agreement with the TPR results. It has been reported in the literature that the Ce/Ni atomic ratio affects the amount of nickel that is incorporated into the ceria lattice [40].

4.2. About the reasons of the different catalytic behavior

The catalytic behavior of the prepared catalysts can be reasonably explained through the above interpretation. In granulated samples, NiO is highly dispersed and with a strong interaction with the support, alumina, which is reflected in a moderate ethane conversion and the highest selectivity toward ethylene. This fact is supported by TPR, XPS and LRS analyses which shows the absence of nickel oxide in bulk form, a very active phase for the ODE reaction but highly unselective.

The presence of the cerium promoter produces important changes in the solid structure by the partial insertion of the Ni cation into the ceria lattice and, hence, by the formation of a Ni–Ce–O solid solution. These "new" nickel species with different chemical environment are more reactive and contribute to activate the ethane at lower temperatures. Hence, the ethane conversion is significantly enhanced in promoted samples.

With the aim to further clarify the role of cerium, an extra alumina-supported catalyst with 15 wt% of total cerium loading (Ce (P)) was prepared. This solid showed very low conversion and low selectivity in the temperature range analyzed. At 450 °C, the ethane conversion and selectivity to ethylene values were 5.2% and 18.5%, respectively, indicating that this component by itself had a very poor performance for the oxidative dehydrogenation of ethane reaction. Therefore, this allowed confirming that the active component is nickel oxide and not the cerium oxide by itself, supporting the above explanations.

Even though the active species formed on the catalytic films are similar, the structured systems present better catalytic performance in terms of ethane conversion and ethylene productivity (by nickel unit mass), compared with those of the granulated forms. This different performance can be explained mainly by:

(i) smaller crystalline domain sizes of active phases, as inferred from Raman spectra,
(ii) a better accessibility of the reagents, due to lower diffusional distances compared with granulated forms, measured by the SEM technique. A higher gas diffusivity for this kind of systems should be taken into account as recently reported by Novák et al. [44],
(iii) the presence of certain components that could contribute to modify the catalytic behavior.

In order to clarify point (iii) and to evaluate the role of these species (mainly chromium) foams coated with calcined Al_2O_3 layers only (550 and 700 °C) were tested under the same reaction conditions as the other catalysts. Both systems showed low ethane conversion, carbon dioxide being the main product. Hence, some active sites for the total oxidation of ethane are present on the alumina layer due to the component migration of the treated foam toward this layer, which could be chromium compounds and iron and manganese spinels [45].

To obtain a better picture of the active elements distribution, EDX experiments were performed. For this purpose, the structured catalysts were cut in three slices. In turn, three regions of each slice were selected for the analysis and four different areas for each region were examined (Fig. 10). The results indicate that chromium was present in all examined zones while iron only appeared rarely and in very few locations. Additionally, manganese was not found in any area. Therefore, taking into account these results it is not possible to conclude that iron or manganese species play a key role.

Through the comparison of the Cr/Ni and Cr/Al ratios measured after the calcination of the Al_2O_3 layer at 550 °C and 700 °C, some differences can be noticed. In fact, the higher calcination temperature generates higher Cr/Ni and Cr/Al ratios on the surface of the catalytic systems. Therefore, there occurs a migration process of some components from the treated foam, which is favored by high temperature treatments. Consequently, the calcination temperature used in the preparation of structured systems affects the migration of components from the metal substrate to the support

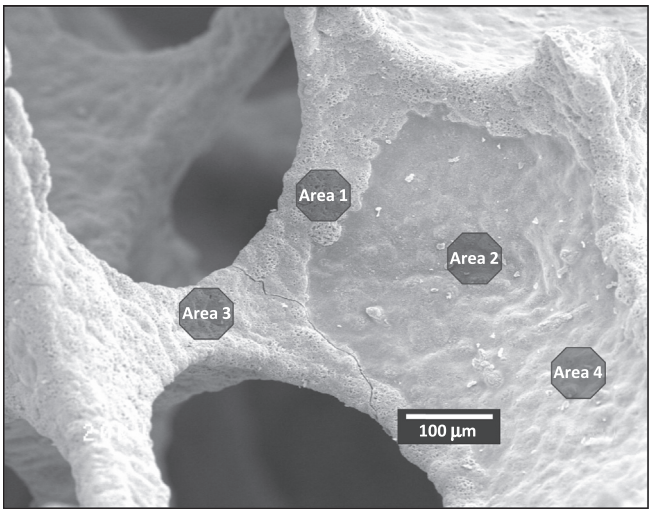

Fig. 10. SEM micrograph of a metallic foam indicating a region selected for the EDX analysis. The four analyzed areas are marked.

and/or to the catalytic coverage. Then, the behavior in the oxidative dehydrogenation reaction is altered, mainly verified by the drop in the selectivity to ethylene (Table 4). This observation shows the negative effect of the increase in chromium amount in the catalytic layer, as verified by EDX analysis (Table 3).

In brief, the structured catalysts (calcined at 550 °C) show a marked increase in catalytic activity but a slightly lower selectivity than granulated formulations for the same reaction temperature. Thus, the global performance is enhanced compared with the granulated forms. The Ni–Ce systems (C550) are more efficient in terms of ethylene productivity than the other catalysts prepared. The main feature of these systems is the homogeneous Ce/Ni ratio in the different sectors of the coverage and the lower Cr/Ni ratio in the catalytic layer.

5. Conclusions

Ni and Ni–Ce/Al_2O_3 granulated catalysts were active and selective for the oxidative dehydrogenation of ethane. The addition of cerium in both atomic ratios (Ce/Ni = 0.11 and 0.25) increased significantly the ethylene productivity by kg of nickel due to the marked increment in ethane conversion. This behavior could be explained by two reasons: (i) the lower nickel oxide crystallite size and (ii) the formation of the solid solution Ni–Ce–O, leading to the generation of new nickel active species.

Catalytic coatings deposited on the foam walls are homogeneously distributed and present high adherence to the substrate. The migration of Cr species from the foam to the catalytic layer is favored by increasing the calcination temperature in the deposition step and modifies the catalytic behavior. The observed changes in the surface composition mainly affect the selectivity to ethylene. Lower temperature treatments reduce the concentration of these components and, hence, minimize the amount of non desired species that favor the ethane total oxidation.

The higher catalytic activity of the structured systems is related to a better utilization of the active sites based on obtaining a thin catalytic film with smaller crystallite sizes of active phases and the improved mass transfer phenomena [44].

The presence of certain components in the coating coming from the base foam (mostly chromium) also contributes to enhance the ethane conversion to some extent. Nevertheless, a higher concentration of chromium species produces a higher increment in ethane conversion but shows a considerable decrease in the selectivity to ethylene that finally causes a lower ethylene productivity. Consequently, doping the Ni–Ce catalysts with chromium would not be a satisfactory approach.

Acknowledgments

The authors wish to acknowledge the financial support received from ANPCyT (Grant PME 8-2003 to purchase the SPECS multitechnique analysis instrument and Grant PME 87-PAE 36985 to purchase the Laser Raman instrument), CONICET and UNL. Thanks are also given to María Fernanda Mori for the XPS measurements and to Elsa Grimaldi for the English language editing.

References

[1] B. Solsona, F. Ivars, A. Dejoz, P. Concepción, M.I. Vázquez, J.M. López Nieto, Supported Ni–W–O mixed oxides as selective catalysts for the oxidative dehydrogenation of ethane, Top. Catal. 52 (2009) 751–757.
[2] F. Cavani, N. Ballarini, A. Cericola, Oxidative dehydrogenation of ethane and propane: how far from commercial implementation?, Catal Today 127 (2007) 113–131.
[3] X. Zhang, J. Liu, Y. Jing, Y. Xie, Support effects on the catalytic behavior of NiO/Al_2O_3 for oxidative dehydrogenation of ethane to ethylene, Appl. Catal. A: Gen. 240 (2003) 143–150.
[4] K.-I. Nakamura, T. Miyake, T. Konishi, T. Suzuki, Oxidative dehydrogenation of ethane to ethylene over NiO loaded on high surface area MgO, J. Mol. Catal. A: Chem. 260 (2006) 144–151.
[5] L. Čapek, L. Vaněk, J. Adam, L. Smoláková, Dehydrogenation of ethane over vanadium, cobalt and nickel based catalysts, Stud. Surf. Sci. Catal. 174 (2008) 1175–1178.
[6] F. Fally, V. Perrichon, H. Vidal, J. Kaspar, G. Blanco, J.M. Pintado, S. Bernal, G. Colon, M. Daturi, J.C. Lavalley, Modification of the oxygen storage capacity of CeO_2–ZrO_2 mixed oxides after redox cycling aging, Catal. Today 59 (2000) 373–386.
[7] H. Vidal, J. Kašpar, M. Pijolat, G. Colon, S. Bernal, A. Cordón, V. Perrichon, F. Fally, Redox behavior of CeO_2–ZrO_2 mixed oxides: II. Influence of redox treatments on low surface area catalysts, Appl. Catal. B: Env. 30 (2001) 75–85.
[8] Y.-P. Fu, S.-H. Hu, B.-L. Liu, Structure characterization and mechanical properties of CeO_2–ZrO_2 solid solution system, Ceram. Int. 35 (2009) 3005–3011.
[9] A. Gurbani, J.L. Ayastuy, M.P. González-Marcos, M.A. Gutiérrez-Ortiz, CuO–CeO_2 catalysts synthesized by various methods: Comparative study of redox properties, Int. J. Hydrogen Energy 35 (2010) 11582–11590.
[10] A. Trovarelli, F. Zamar, J. Llorca, C. de Leitenburg, G. Dolcetti, J.T. Kiss, Nanophase fluorite-structured CeO_2–ZrO_2 catalysts prepared by high-energy mechanical milling, J. Catal. 169 (1997) 490–502.
[11] S. Hosokawa, S. Imamura, S. Iwamoto, M. Inoue, Synthesis of CeO_2–ZrO_2 solid solution by glycothermal method and its oxygen release capacity, J. European Ceram. Soc. 31 (2011) 2463–2470.
[12] Y. Wang, A. Zhu, Y. Zhang, C.T. Au, X. Yang, C. Shi, Catalytic reduction of NO by CO over NiO/CeO_2 catalyst in stoichiometric NO/CO and NO/CO/O_2 reaction, Appl. Catal. B: Env. 81 (2008) 141–149.
[13] A. Iriondo, V.L. Barrio, J.F. Cambra, P.L. Arias, M.B. Guemez, M.C. Sanchez-Sanchez, R.M. Navarro, J.L.G. Fierro, Glycerol steam reforming over Ni catalysts supported on ceria and ceria-promoted alumina, Int. J. Hydrogen Energy 35 (2010) 11622–11633.
[14] R. Pérez-Hernández, A. Gutiérrez-Martínez, J. Palacios, M. Vega-Hernández, V. Rodríguez-Lugo, Hydrogen production by oxidative steam reforming of methanol over Ni/CeO_2–ZrO_2 catalysts, Int. J. Hydrogen Energy 36 (2011) 6601–6608.
[15] M.M. Pakulska, C.M. Grgicak, J.B. Giorgi, The effect of metal and support particle size on NiO/CeO_2 and NiO/ZrO_2 catalyst activity in complete methane oxidation, Appl. Catal. A: Gen. 332 (2007) 124–129.
[16] A.S. Larimi, S.M. Alavi, Ceria–Zirconia supported Ni catalysts for partial oxidation of methane to synthesis gas, Fuel 102 (2012) 366–371.
[17] L. Jalowiecki-Duhamel, A. Ponchel, C. Lamonier, A. D'Huysser, Y. Barbaux, Relationship between structure of $CeNi_XO_Y$ mixed oxides and catalytic properties in oxidative dehydrogenation of propane, Langmuir 17 (2001) 1511–1517.
[18] P. Boizumault-Moriceau, A. Pennequin, B. Grzybowska, Y. Barbaux, Oxidative dehydrogenation of propane on Ni–Ce–O oxide: effect of the preparation method, effect of potassium addition and physical characterization, Appl. Catal. A: Gen. 245 (2003) 55–67.
[19] B. Solsona, P. Concepción, S. Hernández, B. Demicol, J.M. López, Nieto, Oxidative dehydrogenation of ethane over NiO–CeO_2 mixed oxides catalysts, Catal. Today 180 (2012) 51–58.
[20] A. Löfberg, A. Essakhi, S. Paul, Y. Swesi, M.-L. Zanota, V. Meille, I. Pitault, P. Supiot, B. Mutel, V. Le Courtois, E. Bordes-Richard, Use of catalytic oxidation and dehydrogenation of hydrocarbons reactions to highlight improvement of heat transfer in catalytic metallic foams, Chem. Eng. J. 176–177 (2011) 49–56.
[21] A. Löfberg, T. Giornelli, S. Paul, E. Bordes-Richard, Catalytic coatings for structured supports and reactors: VO_x/TiO_2 catalyst coated on stainless steel in the oxidative dehydrogenation of propane, Appl. Catal. A: Gen. 391 (2011) 43–51.
[22] E. Bianchi, T. Heidig, C.G. Visconti, G. Groppi, H. Freund, E. Tronconi, An appraisal of the heat transfer properties of metallic open-cell foams for strongly exo-/endo-thermic catalytic processes in tubular reactors, Chem. Eng. J. 198–199 (2012) 512–528.
[23] Y. Liu, D. Edouard, L.D. Nguyen, D. Begin, P. Nguyen, C. Pham, C. Pham-Huu, High performance structured platelet milli-reactor filled with supported cobalt open cell SiC foam catalyst for the Fischer–Tropsch synthesis, Chem. Eng. J. 222 (2013) 265–273.
[24] E.D. Banús, V.G. Milt, E.E. Miró, M.A. Ulla, Co, Ba, K/ZrO_2 coated onto metallic foam (AISI 314) as a structured catalyst for soot combustion: Coating preparation and characterization, Appl. Catal. A: Gen. 379 (2010) 95–104.
[25] S.R. Kirumakki, B.G. Shpeizer, G.V. Sagar, K.V.R. Chary, A. Clearfield, Hydrogenation of Naphthalene over NiO/SiO_2–Al_2O_3 catalysts: structure–activity correlation, J. Catal. 242 (2006) 319–331.
[26] E. Heracleous, A.F. Lee, K. Wilson, A.A. Lemonidou, Investigation of Ni-based alumina-supported catalysts for the oxidative dehydrogenation of ethane to ethylene: structural characterization and reactivity studies, J. Catal. 231 (2005) 159–171.
[27] A.V. Ghule, K. Ghule, T. Punde, J.-Y. Liu, S.-H. Tzing, J.-Y. Chang, H. Chang, Y.-C. Ling, In situ monitoring of NiO–Al_2O_3 nanoparticles synthesis by thermo-Raman spectroscopy, Mater. Chem. Phys. 119 (2010) 86–92.
[28] W. Wang, Y. Liu, C. Xu, C. Zheng, G. Wang, Synthesis of NiO nanorods by a novel simple precursor thermal decomposition approach, Chem. Phys. Lett. 362 (2002) 119–122.
[29] M.A. Laguna-Bercero, M.L. Sanjuán, R.I. Merino, Raman spectroscopy study of cation disorder in poly- and single crystals of the nickel aluminate spinel, J. Phys. Condens. Matter 19 (2007) 186217–186227.

[30] A. Martínez-Arias, M. Fernández-García, L.N. Salamanca, R.X. Valenzuela, J.C. Conesa, J. Soria, Structural and redox properties of ceria in alumina-supported ceria catalyst supports, J. Phys. Chem. B 104 (2000) 4038–4046.
[31] S. Wang, W. Wang, J. Zuo, Y. Qian, Study of the Raman spectrum of CeO_2 nanometer thin films, Mat. Chem. Phys. 68 (2001) 246–248.
[32] G.W. Graham, W.H. Weber, C.R. Peters, R. Usmen, Empirical method for determining CeO_2-particle size in catalysts by Raman spectroscopy, J. Catal. 130 (1991) 310–313.
[33] S. Kanakaraju, S. Mohan, A.K. Sood, Optical and structural properties of reactive ion beam sputter deposited CeO_2 films, Thin Solid Films 305 (1997) 191–195.
[34] L. Bourja, B. Bakiz, A. Benlhachemi, M. Ezahri, S. Villain, C. Favotto, J.-C. Valmalette, J.R. Gavarri, Structural modifications of nanostructured ceria $CeO_2{\cdot}xH_2O$ during dehydration process, Powder Technol. 215–216 (2012) 66–71.
[35] J.P. Bortolozzi, L.B. Gutierrez, M.A. Ulla, Synthesis of Ni/Al_2O_3 and $Ni–Co/Al_2O_3$ coatings onto AISI 314 foams and their catalytic application for the oxidative dehydrogenation of ethane, App. Catal. A: Gen. 452 (2013) 179–188.
[36] M. Azhar Khan, M.U. Islam, M. Ishaque, I.Z. Rahman, A. Genson, S. Hampshire, Structural and physical properties of Ni–Tb–Fe–O system, Mater. Charact. 60 (2009) 73–78.
[37] M. Prekajski, Z. Dohčević-Mitrović, M. Radović, B. Babić, J. Pantić, A. Kremenović, B. Matović, Nanocrystaline solid solution $CeO_2–Bi_2O_3$, J. European Ceram. Soc. 32 (2012) 1983–1987.
[38] W. Shan, M. Luo, P. Ying, W. Shen, C. Li, Reduction property and catalytic activity of $Ce_{1-X}Ni_XO_2$ mixed oxide catalysts for CH_4 oxidation, Appl. Catal. A: Gen. 246 (2003) 1–9.
[39] N.M. Deraz, Effect of NiO content on structural, surface and catalytic characteristics of nano-crystalline NiO/CeO_2 system, Ceram. Int. 38 (2012) 747–753.
[40] N. Yisup, Y. Cao, W.-L. Feng, W.-L. Dai, K.N. Fan, Catalytic oxidation of methane over novel Ce–Ni–O mixed oxide catalysts prepared by oxalate gel-coprecipitation, Catal. Lett. 99 (2005) 207–213.
[41] S. Xu, X. Yan, X. Wang, Catalytic performances of $NiO–CeO_2$ for the reforming of methane with CO_2 and O_2, Fuel 85 (2006) 2243–2247.
[42] Y.-M. Liu, L.-C. Wang, M. Chen, J. Xu, Y. Cao, H.-Y. He, K.-N. Fan, Highly selective Ce–Ni–O catalysts for efficient low temperature oxidative dehydrogenation of propane, Catal. Lett. 130 (2009) 350–354.
[43] G. Vlaic, R. Di Monte, P. Fornasiero, E. Fonda, J. Kăspar, M. Graziani, Redox property–local structure relationships in the Rh-loaded $CeO_2–ZrO_2$ mixed oxides, J. Catal. 182 (1999) 378–389.
[44] V. Novák, P. Kočí, T. Gregor, J.-S. Choi, F. Štěpánek, M. Marek, Effect of cavities and cracks on diffusivity in coated catalyst layer, Cat. Today 216 (2013) 142–149.
[45] J.P. Bortolozzi, E.D. Banús, V.G. Milt, L.B. Gutierrez, M.A. Ulla, The significance of passivation treatments on AISI 314 foam pieces to be used as substrates for catalytic applications, Appl. Surf. Sci. 257 (2010) 495–502.